



Article

Rapid Self-Assembly of Polymer Nanoparticles for Synergistic Codelivery of Paclitaxel and Lapatinib via Flash NanoPrecipitation

Shani L. Levit 1, Hu Yang 1,2,3 and Christina Tang 1,*

- Chemical and Life Science Engineering Department, Virginia Commonwealth University, Richmond, VA 23284, USA; levitsl@vcu.edu (S.L.L.); hyang2@vcu.edu (H.Y.)
- Department of Pharmaceutics, Virginia Commonwealth University, Richmond, VA 23298, USA
- Massey Cancer Center, Virginia Commonwealth University, Richmond, VA 23298, USA
- * Correspondence: ctang2@vcu.edu

Received: 17 February 2020; Accepted: 18 March 2020; Published: 20 March 2020



Abstract: Taxol, a formulation of paclitaxel (PTX), is one of the most widely used anticancer drugs, particularly for treating recurring ovarian carcinomas following surgery. Clinically, PTX is used in combination with other drugs such as lapatinib (LAP) to increase treatment efficacy. Delivering drug combinations with nanoparticles has the potential to improve chemotherapy outcomes. In this study, we use Flash NanoPrecipitation, a rapid, scalable process to encapsulate weakly hydrophobic drugs (logP < 6) PTX and LAP into polymer nanoparticles with a coordination complex of tannic acid and iron formed during the mixing process. We determine the formulation parameters required to achieve uniform nanoparticles and evaluate the drug release in vitro. The size of the resulting nanoparticles was stable at pH7.4, facilitating sustained drug release via first-order Fickian diffusion. Encapsulating either PTX or LAP into nanoparticles increases drug potency (as indicated by the decrease in IC-50 concentration); we observe a 1500-fold increase in PTX potency and a six-fold increase in LAP potency. When PTX and LAP are co-loaded in the same nanoparticle, they have a synergistic effect that is greater than treating with two single-drug-loaded nanoparticles as the combination index is 0.23 compared to 0.40, respectively.

Keywords: Flash NanoPrecipitation; polymer nanoparticle; codelivery; combination therapy; drug synergy; ovarian cancer; nanomedicine

1. Introduction

Ovarian cancer remains one of the most difficult cancers to treat due to late-stage diagnosis and its highly malignant nature [1]. Chemotherapies such as Taxol, a formulation of paclitaxel (PTX), remains to be one of the most widely used cancer treatments, particularly for recurring ovarian carcinomas following surgery [1–3]. The mechanism of action for PTX is binding to the β -subunit of tubulin at two sites, which stabilizes the tubulin polymers preventing cytoskeletal rearrangement for cellular function [4–6]. Stabilizing tubulin results in cell cycle arrests in the G_2/M phase [6]. However, there are many challenges with the use of Taxol. There are severe systemic side effects associated with PTX treatment such as low blood pressure, risk of infection, the formation of blood clots, and neurotoxicity [7–9]. Additionally, PTX is poorly water-soluble and has low permeability which limits drug efficacy due to low drug concentrations reaching the tumor site [10]. Clinically, PTX is used in combination with other drugs to increase the efficacy of treatment by targeting multiple pathways [11–13].

Paclitaxel is often used in combination with lapatinib (Tykerb, LAP), a class of tyrosine kinase inhibitors [14–17]. Several studies observed an increase in drug efficacy in terms of tumor cell death

Nanomaterials **2020**, 10, 561 2 of 17

and decrease in tumor volume when PTX and LAP were used in combination [15,18]; in some cases, a synergetic effect was observed [19]. However, combination treatment required premedication before injection, i.e., complex treatment regimens with multiple methods of administration [20,21]. Formulation of drug combinations in nanoparticles could overcome low solubility and permeability of the drugs to deliver an effective drug dosage to the tumor site and simplify drug regimens to improve patient adherence, while decreasing side effects [7,22,23].

Co-encapsulation of PTX and LAP may improve the co-localization of the drugs in the tumor tissue and increase drug efficacy [7,24–27]. For example, PTX and LAP have been co-formulated in a core-shell structure using polymer micelles. Lapatinib was conjugated to a PEGylated block copolymer and formulated into micelles encapsulating PTX in the core. Interestingly, formulation into the polymer micelles increased the potency of the PTX as indicated by a two-fold decrease in the half-maximal inhibitory concentration (IC-50) concentration in certain types of breast cancer [25]. Although the increase in potency via formulation into nanoparticles is exciting, this approach requires multiple steps and covalent modifications of LAP which results in the formation of a new compound, requiring further testing for FDA approval, a costly and time-consuming process [28].

Nanoparticle formulations co-encapsulating PTX and LAP without the chemical modification of LAP have also been considered [7,24–27,29]. Vergara et al. co-encapsulated LAP and PTX in polyelectrolyte nanoparticles by the sonication-assisted layer-by-layer (SLBL) technique. To formulate these nanoparticles, PTX-chitosan nanoparticles were first formed, followed by the sequential deposition of alginic acid and chitosan coatings. Lapatinib was co-deposited with chitosan to achieve nanoparticles with a PTX core and LAP shell. The core-shell nanoparticles showed a significant decrease in cell viability in vitro compared to PTX-loaded nanoparticles and free PTX [7]. While the results are promising, the formulation of the nanoparticles was time intensive as each deposition of each layer required 20–45 min.

Co-loading both LAP and PTX in the nanoparticle core has been achieved using lipopolymer [24] or Pluronic F127 polymeric micelles [30]. Formulation using the Pluronic F127 suppressed tumor cell proliferation and decreased IC-50 by 10-folds relative to the free drug combination treatment of PTX and LAP [30]. These nanoparticles provide the basis for further improvements of drug combinations; however, the formulation method is challenging to scale up [31]. Furthermore, the drug effect when co-delivering drugs in nanoparticle form in terms of synergy is not well established.

In this study, we extend the use of Flash NanoPrecipitation (FNP) to PTX and LAP by leveraging in situ coordination complexation of tannic acid and iron. Flash NanoPrecipitation enables the rapid, scalable formulation of drug combinations [32]. However, this method has generally been limited to highly hydrophobic materials (logP > 6) [33]. Encapsulating PTX and LAP using FNP is challenging due to their relatively weak hydrophobicity (PTX, logP = 3.2 and LAP, logP = 5.4). We encapsulate drugs (logP < 6) via in situ coordination complex formation of tannic acid—iron (TA–Fe) and stabilization with an amphiphilic block copolymer. Our focus is on understanding how incorporating multiple drugs affects nanoparticle self-assembly. Based on our understanding, we establish the formulation parameters to form PTX NPs, LAP NPs, and PTX–LAP NPs with comparable sizes (~100 nm in diameter). We perform initial drug release studies in vitro, focusing on the release of PTX. We evaluate the potency of the nanoparticles in vitro using an ovarian cancer cell line OVCA-432. The core of our preliminary in vitro evaluation is based on IC-50 values; the effect of co-encapsulating the drugs in terms of synergy using the combination index is analyzed.

2. Materials and Methods

2.1. Materials

HPLC grade tetrahydrofuran (THF), dimethyl sulfoxide (DMSO), acetonitrile, and Tween 80 were purchased from Fisher Scientific (Pittsburg, PA, USA). ACS grade tannic acid (TA) and ACS grade iron (III) chloride hexahydrate (97%) were purchased from Sigma-Aldrich (St. Louis, MO, USA). Paclitaxel

Nanomaterials **2020**, *10*, 561 3 of 17

(PTX, >98%) and lapatinib (LAP, >98%) were obtained from Cayman Chemical Company (Ann Arbor, MI, USA); phosphate-buffered saline without calcium and magnesium was purchased from Lonza (Basel, Switzerland). Polystyrene-b-polyethylene glycol (1600-b-500 g/mol) (PS-b-PEG) was obtained from Polymer Source (Montreal, Quebec, Canada) and was purified by dissolving in THF (~40 °C) and precipitating into diethyl ether then dried by vacuum for two days as previously described [34].

2.2. Cell Culture

Ovarian cancer cell line OVCA-432 was a kind gift from Dr. Xianjun Fang from Virginia Commonwealth University. The OVCA-432 cells were cultured in RPMI-1640 media containing 2 mM L-glutamine (ATCC, Manassas, VA, USA) supplemented with 10% Fortified Bovine Calf Serum (FBS, HyClone Cosmic Calf Serum, Fisher Scientific, Pittsburg, PA, USA), 100 U/mL penicillin and 100 μ g/mL streptomycin (Gemini Bio-Products, West Sacramento, CA, USA), and cultured at 37 °C at 5% CO₂. The cells were passaged once a week.

2.3. Nanoparticle Formulation

Flash NanoPrecipitation (FNP) was used to prepare polymer-based nanoparticles encapsulating the anti-cancer drugs with a hand-operated confined impinging jet (CIJ) mixer with dilution as previously described [35,36]. Four nanoparticles were formulated that either encapsulated the TA–Fe complex (TA–Fe NPs), PTX (PTX NPs), LAP (LAP NPs), or both PTX and LAP (PTX–LAP NPs).

To self-assemble the nanoparticles, PS-b-PEG, TA (4 mg/mL), and one or more of the drugs (PTX and LAP) were dissolved in a water-miscible organic solvent (e.g., THF or DMSO) by sonication (\sim 40 °C) for 10 min to formulate the organic stream. The organic stream was rapidly mixed with the Fe³⁺ (aq., 1 mg/mL) at equal volumes, typically 1 mL, in the CIJ mixer. The effluent from the mixer was immediately diluted in 1X PBS at pH 7.4 for a final organic solvent/water ratio of 1:9 by volume. The drug concentration in the organic stream of PTX and LAP was varied from 0.5 mg/mL to 2 mg/mL; the block copolymer concentration was varied relative to the core material. Specifically, the core material was considered the TA and Fe³⁺ for the TA–Fe NPs, and for the drug-loaded nanoparticles it was determined as TA and the drugs encapsulated. The ratio of the PS-b-PEG to the core material was varied between 1:1 and 2:1 by mass.

Within 24 h of formulation, the nanoparticles were filtered to remove the organic solvent, unencapsulated drug(s), and excess TA and Fe $^{3+}$ with Amicon Ultra-2 Centrifugal filters (Amicon Ultracentrifuge filter (Ultracel 50K, 50,000 NMWL), Merck Millipore Ltd., Burlington, MA, USA) by centrifuging at 3700× g rpm for ~15–30 min (5804 R 15 amp version, Eppendorf, Hamburg, Germany). The nanoparticle pellet was resuspended with 1X PBS to a nominal concentration of ~25 mg/mL of total solids and stored at ~4 °C. The nanoparticles were used within 5 days of the FNP to ensure there was minimal change in particle size and drug loss.

2.4. Nanoparticle Characterization

The size, polydispersity (PDI), and zeta potential of the nanoparticles were characterized immediately after FNP and after filtration using dynamic light scattering (Malvern Zetasizer ZS, Malvern Instruments Ltd., Malvern, United Kingdom). The nanoparticle size and polydispersity index (PDI), a measure of uniformity, were measured by averaging 4 measurements at a scattering angle of 173°. Nanoparticles populations with a PDI of less than 0.400 were considered uniform [37]. The nanoparticle size stability at 4 °C was observed by measuring size and PDI for up to 3 weeks after formulation. The concentration of the nanoparticle dispersion following filtration was determined by thermogravimetric analysis (TGA) (Pyris 1 TGA, Perkin Elmer, Waltham, MA, USA).

Transmission electron microscopy (TEM) samples were prepared by diluting the filtered nanoparticle dispersions with DI water 1:20 by volume ratio and pipetting 5 μ L three times onto a TEM grid with Formvar/Carbon support films (200 mesh, Cu, Ted Pella, Inc., Redding, CA, USA) and dried

Nanomaterials **2020**, 10, 561 4 of 17

under ambient conditions. Dilution was necessary to prevent aggregation during drying. The samples were imaged with a JEOL JEM-1230 (JEOL USA, Inc., Peabody, MA, USA) at 120 kV.

To determine the drug content of the nanoparticles, acetonitrile (1.8 mL) was added to nanoparticles (50 μ L) filtered with Amicon filter, as previously described, and the sample was vortexed so that the nanoparticles would disassemble. The sample was centrifuged at 10,000× g rpm for 6 min, and then the supernatant was collected for reverse-phase high-performance liquid chromatography (RP–HPLC) (1260 HPLC with Quaternary Pump and UV–Vis Diode Array Detector, Agilent, Santa Clara, CA, USA) fitted with a Luna® 5 μ m C18 100 Å, LC Column 250 × 4.6 mm (Phenomenex, Torrance, CA, USA). The sample was eluted with degassed acetonitrile and water gradient at a flow rate of 1 mL/min (0–1 min at 80:20, 1–6 of ramp up to 0:100, 6–8 min at 0:100, and ramp down to 80:20 between 8 and 9 min). PTX was measured at a wavelength of 228 nm with a retention time of ~8 min and LAP was measured at 332 nm with a retention time of ~9 min. The concentration of each drug was determined by comparing the peak areas with the standard calibration curve. Encapsulation efficiency (EE%) and drug loading (DL%) were calculated based on Equations (1) and (2), respectively, and the values reported are the average and standard deviation of three trials.

Encapsulation efficiency (EE%) =
$$\frac{Mass\ of\ drug\ encapsulated}{Initial\ mass\ of\ drug} \times 100\%$$
 (1)

$$Drug \ loading \ (DL\%) = \frac{Mass \ of \ drug \ encapsulated}{Total \ nanoparticle \ mass} \times 100\% \tag{2}$$

2.5. Nanoparticle Drug Release In Vitro

To measure the drug release, 500 μ L of concentrated nanoparticle dispersion was loaded into a 7000 MWCO dialysis unit (Slide-A-Lyzer® MINI Dialysis Unit, Thermo Scientific, Waltham, MA, USA) and incubated in 0.5% Tween 80 in PBS at pH 7.4 at 37 °C, which was replaced every day of the experiment. Samples (32 μ L) at 0 h, 3 h, 6 h, 24 h, 48 h, day 4, day 6, and day 10 were taken from the nanoparticle dispersion and the remaining drug concentration was determined by RP–HPLC as previously described. Three replicates of each drug-loaded nanoparticle dispersion were tested.

2.6. Cytotoxicity

OVA-432 cells were seeded at a density of 15×10^3 cell/well in a 96-well plate containing 100 µL of complete medium. The cells were incubated at 37 °C in 5% CO₂ overnight. Then the media was replaced with 100 μL medium containing free drugs or nanoparticles and treated for 48 h. Stock solutions of free drug were prepared by dissolving PTX (12 mg/mL) or LAP (5 mg/mL) in DMSO and sonicating for 5 min. Then, the drugs were diluted with complete media and serial dilutions were performed to achieve concentrations between 200 and 0.0002 μg/mL. Additional DMSO was added for a final DMSO concentration of 2% v/v. The nanoparticles were concentrated with Amicon filters (50 kDa MWCO) as previously described and the nanoparticle pellet was diluted with 1X PBS. The PTX NPs and LAP NPs were individually concentrated to 1,000 µg/mL of drug. The PTX-LAP NPs were concentrated to 500 µg/mL relative to PTX. The nanoparticle-loaded medium was prepared by diluting the stock nanoparticle dispersion with complete media and performing serial dilutions for final concentrations between 200 and 0.0002 µg/mL. The cells were also treated with complete media and 2% v/v DMSO media as controls for comparison. There were 6 replicates for each experimental condition. After 48 h, the cell viability was measured with WST-1 assay (Sigma-Aldrich, St. Louis, MO, USA) according to manufacturing instructions. Briefly, the drug-loaded medium was removed and 100 μL of RPMI-1640 with Phenol Red (Fisher Scientific, Pittsburg, PA, USA) containing 10% WST-1 solution was added to each well as well as to 6 empty wells. The cells were incubated between 45 and 90 min until there was a visible color change to a golden-yellow or the absorbance of control wells reached at least 0.700 measured with a microplate reader (VersaMax ELISA microplate reader, Nanomaterials **2020**, 10, 561 5 of 17

Molecular Devices, San Jose, CA, USA) at a wavelength of 440 nm with background subtraction of 640 nm. The cell viability was determined by subtracting the background noise (wells containing only 10% WST-1 in media) from the samples and then dividing the sample absorbance by the average absorbance of the untreated wells. The relative cell viability was expressed as a percentage of the untreated cells with a mean \pm standard deviation of six replicates.

2.7. Cell Cycle Analysis by Flow Cytometry

The cells were seeded at a density of 20×10^4 cells/mL in a 35 mm petri dish containing 3 mL of complete media. The cells were incubated at 37 °C and 5% CO₂ until 90% confluence and the media was replaced every 2 days. The cells were treated with either free PTX, free LAP, PTX NPs, LAP NPs at the IC-50 concentration, or left untreated for 48 h at 37 °C. After 48 h treatment, the cells were stained with Propidium Iodide (PI Flow Cytometry Kit, Abcam, Cambridge, MA, USA) for flow cytometry according to the manufacturer's instructions. Briefly, the cells were trypsinized and the aspirated medium and PBS were collected to minimize cell loss. The cells were centrifuged at $700 \times g$ for 5 min as necessary. The cells were washed with 1X PBS and fixed with 66% ethanol by slowly adding ethanol to PBS during vortexing. The cells were stored in ethanol at 4 °C for at least 2 h and up to 4 days. The cells were centrifuged and washed with PBS to remove the ethanol. The 1× Propidium Iodide and RNase solution was prepared immediately prior to use by mixing 5% v/v of 20× Propidium Iodide and 0.05% v/v 200X RNase in 1X PBS. Then the cells were resuspended in 200 μL/500,000 cells of 1X Propidium Iodide and RNase solution and incubated in the dark at 37 °C for 30 min. Prior to flow cytometry, the cell samples were stored on ice and filtered through a cell strainer (Falcon Test Tube with Snap Cap, Fisher Scientific, Pittsburg, PA, USA). Flow cytometry was performed on a BD FACSCanto™ II Analyzer (BD Biosciences, San Diego, CA, USA) and 10,000 cells were analyzed at an excitation of 488 nm and emission of 670 nm. The samples were analyzed in triplicate.

3. Results and Discussion

3.1. Nanoparticle Preparation and Characterization

Flash NanoPrecipitation (FNP) is a well-established polymer-directed self-assembly method for preparing size-tunable nanoparticles encapsulating highly hydrophobic molecules (logP > 6). Since nanoparticle self-assembly involves adsorption of the hydrophobic block of the block copolymer to a precipitating core material, this process has generally been limited to highly hydrophobic materials with a logP of six or greater [32,33]. Since PTX is not sufficiently hydrophobic to form stable particles via FNP directly [38], we explore an alternative approach in which we encapsulate PTX (logP = 3.2) and LAP (logP = 5.4) using a pH-labile, tannic acid—iron (TA—Fe) based nanoparticle platform [35].

To prepare TA–Fe based nanoparticles, FNP was performed by mixing drug(s), dissolving TA and PS-b-PEG in a water-miscible (THF or DMSO) organic solvent with iron (III) chloride dissolved in water in a confined impinging jet mixer. The effluent from the mixer was quenched in a bath of PBS, pH 7.4, conditions under which the TA–Fe coordination complex is expected to be insoluble. Upon rapid mixing, the TA and Fe³⁺ form an insoluble coordinate complex which co-precipitates with the drug(s) forming the particle core. Precipitation of the core materials is arrested by adsorption of the hydrophobic block of the block copolymer and the PEGylated end of the block copolymer sterically stabilizes the nanoparticle in dispersion (Figure S1). The dispersions appeared red which is consistent with the tris-complex of TA and iron expected at pH 7.4 [31,39]. Nanoparticles encapsulating the TA–Fe complex (TA–Fe NPs) are 109 ± 5 nm (Figure S2) with a zeta potential of -21.4 ± 2.1 mV consistent with other PEGylated nanoparticles [33,40].

Our initial goal was to achieve uniform PTX-loaded nanoparticles on the order of 100 nm to allow for passive targeting [41]. We examined the effect of organic solvent selection, total solids concentration, ratio of the block copolymer to core materials, and drug concentration on the ability to make uniform particles and resulting nanoparticle size.

Nanomaterials **2020**, 10, 561 6 of 17

Two water-miscible organic solvents were considered, THF and DMSO, as the block copolymer; TA, LAP, and PTX were sufficiently soluble for the self-assembly of nanoparticles via FNP. However, when DMSO was used for the organic stream, a visible red-purple precipitate formed immediately upon mixing in the reservoir. With THF, stable PTX-loaded nanoparticle dispersions were achieved with a zeta potential of -22.1 ± 2.1 mV and no precipitate was observed. These results suggest that co-precipitation of PTX and the TA–Fe complex and the rate of PS-b-PEG self-assembly is more appropriately matched using THF as a solvent than DMSO as a solvent. Thus, THF was used as a solvent in all further experiments.

To further tune the size of the PTX-loaded particles, we examined the effect of other formulation parameters. At a total solid concentration of 18 mg/mL in the streams and above, there are two size populations in the intensity weighted distribution with peak diameters of ~30 nm and ~100 nm. The population with a hydrodynamic diameter of ~30 nm can be attributed to empty block copolymer micelles [35,42] produced with the PTX-loaded nanoparticles of ~100 nm (Table 1). The inability to form uniform particles at high concentrations has been previously observed and could be attributed to a limited affinity between stabilizer and TA–Fe precipitates at high iron concentrations [35].

Ratio of BCP:Core	PTX Concentration (mg/mL)	Size 1 (nm)	Size 2 (nm)	PDI
2:1	1	107 ± 2	32 ± 1	0.275 ± 0.009
2:1	2	113 ± 6	31 ± 1	0.372 ± 0.012
1:1	1	170 ± 33	0	0.142 ± 0.053
1.5:1	1	128 ± 7	0	0.244 ± 0.034
2:1	1	111 ± 10	0	0.255 ± 0.021
2:1	2	117 ± 3	20 ± 1	0.268 ± 0.009
2:1	1	111 ± 10	0	0.255 ± 0.021
2:1	0.5	134 ± 42	0	0.232 ± 0.145
	2:1 2:1 1:1 1.5:1 2:1 2:1	BCP:Core (mg/mL) 2:1 1 2:1 2 1:1 1 1.5:1 1 2:1 1 2:1 2 2:1 1	BCP:Core (mg/mL) Size 1 (nm) 2:1 1 107 ± 2 2:1 2 113 ± 6 1:1 1 170 ± 33 1.5:1 1 128 ± 7 2:1 1 111 ± 10 2:1 2 117 ± 3 2:1 1 111 ± 10	BCP:Core (mg/mL) Size 1 (nm) Size 2 (nm) 2:1 1 107 ± 2 32 ± 1 2:1 2 113 ± 6 31 ± 1 1:1 1 170 ± 33 0 1.5:1 1 128 ± 7 0 2:1 1 111 ± 10 0 2:1 2 117 ± 3 20 ± 1 2:1 1 111 ± 10 0

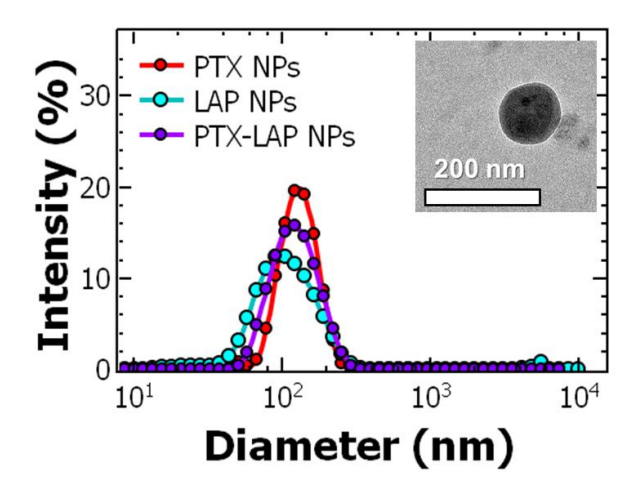
Table 1. Summary of paclitaxel nanoparticle formulations.

The average \pm standard deviation of 3 replicates of Flash NanoPrecipitation (FNP) are reported.

To improve particle uniformity, we next examined the ratio of the block copolymer to core materials (BCP: core with the core defined as a concentration of TA and PTX in the formulation) at reduced total solids concentration. Specifically, three BCP: core ratios, i.e., 1:1 1.5:1, and 2:1, were studied with a total solid concentration of less than 16 mg/mL. All three ratios produced uniform nanoparticles with a PDI < 0.400. At a 1:1 BCP: core ratio, the particles were 170 ± 33 nm. Increasing the amount of block copolymer from a 1:1 to 2:1 BCP: core ratio produced a 35% decrease in particle size (Table 1) and, for the 2:1 BCP: core ratio, uniform PTX-loaded particles with a hydrodynamic diameter of 117 ± 3 nm were achieved. TEM confirmed the nanoparticles were spherical and the size was consistent with DLS (Figure S3A). This trend has been attributed to an increase in the rate of self-assembly relative to the rate of core growth, limiting the growth of the core before it is kinetically stabilized. These results are comparable to FNP systems using hydrophobic core materials (logP > 6) in which the particle size can be tuned by varying the ratio of the block copolymer to the core [32,39].

Thus, we next investigated the effect of PTX concentration to maximize the drug loading in the nanoparticle while maintaining uniform, ~100 nm nanoparticle formulations (Figure 1). We varied the PTX concentration from 0.5 to 2 mg/mL in the organic stream. Increasing the PTX concentration to 2 mg/mL resulted in two size populations with peak diameters of ~100 nm and ~20 nm (Table 1) possibly due to a mismatch time scales of complexation/precipitation and block copolymer micellization at higher concentrations of the drug. The highest concentration that we used that resulted in uniform PTX-loaded particles was 1 mg/mL.

Nanomaterials 2020, 10, x FOR PEER REVIEW



FigliguteRepresentation dynamical instruction of the control of the properties of the properties of the control of the properties of the properties of the control of the c

In paramed betwith normal gives 173 alonds dopanders; ides also cases from 45 Properties with the simple parametrister via the parametrister via the parametrister of them in alience ter.

Similite to TRT, to the beal do representation bear 36 graffed. In the extreme structed in the constitution with peak diameter ~30 nm and ~100 nm due to the constitution of order to the constitution of the extreme structed in the structed diameter and the constitution of the constitution of the extreme structed in the extreme

Table 2. Summary of lapatinib nanoparticle formulations.

Total Solids (mg/mL)	Summary O Ratio of BCP:	Lapatinib nanoparticle form	ulations Size 2 (nm)	PDI
16Total Solids	Ratið:bf	Size 1 (nm) $_{06}^{91 \pm 10}$ 2 (nm)	0	0.214 ± 0.038
36 (mg/mL)	BCP:2÷bre		26 PPI	0.288 ± 0.004
10.5 16	2: 1 :1	$91 \pm 10^{134} \pm 8 0$	$0.21^{\circ}4 \pm 0.038$	0.255 ± 0.012
15.3 36	2:1	$106 \pm 5^{126} \pm \frac{7}{2}6 \pm 4$	0.288 ± 0.004	0.380 ± 0.037
$10.5^{\text{The average}} \stackrel{+}{1:1}^{\text{standard deviation } gf 3} \stackrel{+}{1:0}^{\text{standard deviation } gf 3} \stackrel{+}{1:0}^{\text{replicates of FNP are reported}} 0.255 \stackrel{+}{=} 0.012$				

Next, we investigated the effect of LAP concentration to maximize the drug loading in the nanoparticle while maintaining uniform size distributions (diameter ~ 100 nm). At LAP concentrations

2 Ng/n, we anovestigates where after used and color and to 3 harm. Eighte \$4 ug Toesta gest the are nationally with the results about the distribution of the statistical and provided with the provided with the statistical and provided with the provided with the statistical and the sore that some constitutions are sufficiently and provided with the sore that the sore that some constitutions are sufficiently and the sore that some constitution of the sore weakly distributions are sufficiently and the sore that some constitution as well as the affinity of the stabilizer and the core that can result in the formal conversable of the stabilizer and the core that can result in the formal conversable of the stabilizer and the core that can result in the formal conversable and the sore of the stabilizer and the core that can result in the formal conversable and the sore of the stabilizer and the core that can result in the formal conversable and the sore of the stabilizer and the core that can result in the formal conversable and the sore of the stabilizer and the core that can result in the formal conversable and the sore of the stabilizer and the core that can result in the formal conversable and the sore of the stabilizer and the core that can result in the formal conversable and the sore of the stabilizer and the core that can result in the formal conversable and the sore of the stabilizer and the core that can result in the formal conversable and the sore of the stabilizer and the core that can result in the formal conversable and the sore of the stabilizer and the core that can result in the formal conversable and the sore of the stabilizer and the core that can result in the formal conversable and the sore of the stabilizer and the core that can result in the formal conversable and the sore of the stabilizer and the core that can result in the formal conversable and the sore of the stabilizer and the core that can result in the sore of the stabilizer and the sore of the stabilizer and the sore of the sore of the

LAP NPs). Based on the findings from formulating PTX NPs and LAP NPs, we first focused on drug concentration using THF as the organic solvent. Using a drug concentration of 1 mg/mL PTX and 1

Nanomaterials **2020**, *10*, 561 8 of 17

1 mg/mL LAP (a total drug concentration of 2 mg/mL), nanoparticles with multiple two size populations (peak diameters of 119 \pm 28 nm and 22 \pm 3 nm) were observed. When the total drug concentration was decreased to 1 mg/mL (0.5 mg/mL each of PTX and LAP), uniform nanoparticles were produced at 115 \pm 3 nm (Table S1). These results are comparable with PTX NPs and LAP NPs where a maximum drug concentration of 1 mg/mL could be used in the formation of monodispersed nanoparticles. To maximize the drug loading, a BCP: core ratio of 1:5:1 was used. TEM confirms the particles are spherical and the particle size is consistent with DLS (Figure 1 and Figure S3C). Additionally, the nanoparticle size and polydispersity were unaffected by the filtration process (Table S2). Nanoparticle size was stable for up to two weeks after FNP when stored at 4 °C (Table S3).

Following FNP, the drug concentration in the resulting dispersions was determined by HPLC after disassembling the nanoparticles with acetonitrile. From the drug concentration, the encapsulation efficiency and drug loading of PTX and LAP were determined. The encapsulation efficiency of the drug is the amount of drug encapsulated compared to the nominal amount in the formulation. The drug loading of PTX and LAP in the single-drug-loaded nanoparticles were similar (Table 3) and comparable to previous literature using polymer micelles [27,43]. For the single-drug-loaded nanoparticles, the encapsulation efficiency PTX and the LAP were $37.6\% \pm 14.4\%$ and $25.0\% \pm 1.5\%$, respectively, which are comparable to previous reports using polymer micelles [43]. Interestingly, in the co-loaded nanoparticles, the encapsulation efficiency of PTX increases from $37.6\% \pm 14.4\%$ to $67.0\% \pm 2.2\%$ while the encapsulation efficiency for LAP in PTX-LAP NPs remained the same as the LAP NPs (Table 3). This result could be attributed to a more hydrophobic core environment in the presence of LAP facilitating encapsulation of PTX. Due to the selective increase in encapsulation efficiency of PTX in the presence of LAP, the drug loading of PTX was 2.7-fold higher than the LAP loading (2.11% \pm 0.50% compared to 0.79% \pm 0.49%) despite using equal amounts of each drug during mixing (0.5 mg/mL of each). Notably, these drug concentrations are comparable to previous studies micelles [27,43].

Samples _	Encapsulation Efficiency (EE%)		Drug Loading (DL%)	
	PTX	LAP	PTX	LAP
PTX NPs	37.6 ± 14.4	-	3.11 ± 1.88	-
LAP NPs	-	25.0 ± 1.5	-	1.82 ± 0.71
PTX-LAP NPs	67.0 ± 2.2	25.9 ± 3.5	2.11 ± 0.50	0.79 ± 0.40

Table 3. Encapsulation efficiency and drug loading of nanoparticles.

The average \pm standard deviation of 3 replicates of FNP are reported.

3.2. Drug Release

As a first step to understanding the in vitro drug release rates of PTX and LAP from nanoparticles, dialysis was performed with PBS at pH 7.4 with Tween 80 similar to previous studies [44–47]. Examining the PTX-loaded nanoparticles, a burst release was observed within the first six hours at which \sim 20% of PTX was released. After six hours, the burst release was followed by sustained PTX release and the drug release plateaued at \sim 40% on day six (Figure 2A). In comparison, \sim 25% of LAP released from LAP-loaded NPs in the first three hours (\sim 25%). Following the burst release, the sustained release of LAP release over six days was observed with \sim 35% total drug release achieved (Figure 2B).

PTX release from the co-loaded nanoparticles was comparable to the single-drug-loaded nanoparticles with burst release in the first six hours and cumulative drug release at day six of \sim 40%. We examined the drug release kinetics of PTX from single-drug and co-loaded nanoparticles and fitted it to the Korsmeyer–Peppas diffusion model (Equation (3)) [48,49]

$$\frac{M_t}{M_{\infty}} = at^n \tag{3}$$

where the M_t is the drug release at time, t, M_{∞} is maximum drug release, and a is the release rate. The diffusion expanent the adjectenined has adopt, the sits and described the drug release metherisms t^2 late. The history point t^2 is a release of the adject the analysis of the anal

differentive of the Nasquesch are observed to the superscript of the sum of t

This pretication of lines become the PTT with Police that proper and earness in an entire telespoint. AP between being that pretices the teleses in a compare telese in superpretation and compare telesistic. This present the superpretation of and compare telesistic. This present telesistic in superpretation of and compare telesistic. This present telesistic in the color of the present that the present the

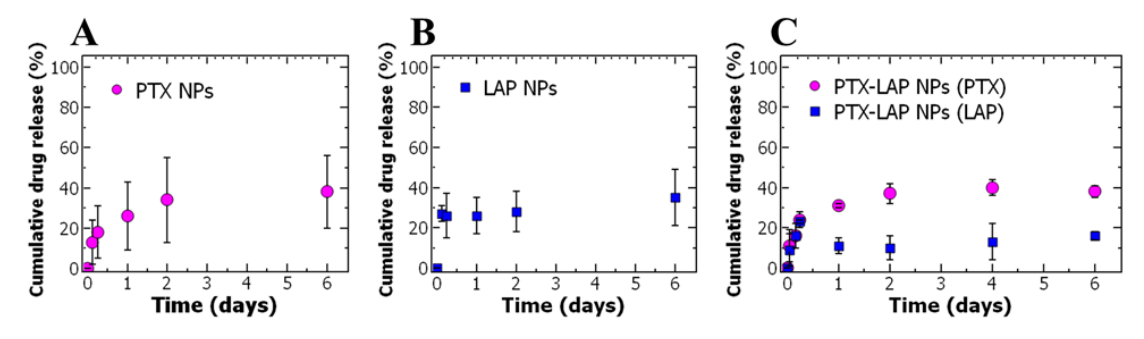


Figure 2. The trum unitivatide was rightered as profited by the trumbal property of the proper

3.3. Assessing Drugfleffigg of Str Siles to Drug an openacticles

Firting!! Inthereffices so fithe manoparticle dispersions was assessed in the withen originary cerestically. GAC4A24522 espicially weed the Interaction that in the other engentration that reduces reduced he is bill than 160% as own assumed so he of the cell this bill than 160% as own assumed so he is bill than 160% as own assumed so he is bill than 160% as own assumed extension the cell this bill than 160% as own assumed extension the cell this bill than 160% as own as the cell this bill than 160% as own as the cell this bill than 160% as own as the cell this construction that are the cell than 160% as own as the cell that t

Next, we compared the potency of the nanoparticles compared to the free drug at the equivalent free drug concentration. We note at the concentrations of nanoparticles used, the (TA–Fe NPs) alone

Nanomaterials **2020**, *10*, 561 10 of 17

Next, we compared the potency of the nanoparticles compared to the free drug at the equivalent free drug concentration. We note at the concentrations of nanoparticles used, the (TA–Fe NPs) alone did not induce cytotoxic effects and the IC-50 was reproducible with OVCA-432 cells (Table S5). Encapsulating the PTX shifts the dose–response curve to lower concentrations compared to free PTX (Table S6) indicating an increase in potency upon encapsulation. A similar trend was observed for LAP (Figure S5). Interestingly, the dose–response curve of PTX NPs and LAP NPs plateaued at ~20% cell viability. At low drug concentrations, the TA in the nanoparticle could counter the effects of the drugs by inducing an antioxidant effect and eliminate free radicals produced with the anticancer drugs [56,57].

Specifically, the IC-50 concentration decreases from $70.6 \pm 5.1 \,\mu\text{g/mL}$ for free PTX to $0.040 \pm 0.003 \,\mu\text{g/mL}$ when encapsulated (p < 0.05) (Table 4). A similar result was observed for LAP; upon encapsulation, there was a nearly six-fold increase in potency as the IC-50 decreased from $4.6 \pm 1.3 \,\mu\text{g/mL}$ for the free drug to $0.80 \pm 0.26 \,\mu\text{g/mL}$ when formulated into nanoparticles (p < 0.05) (Table 4). While decreases in IC-50 concentration compared to the free drug form have been observed in other polymer nanoparticle formulations [24,58,59] and are not fully understood, the 1500-fold increase in PTX potency in this nanoparticle is noteworthy. The significant increase in PTX potency in the TA–Fe could be attributed to several contributing factors including sustained release over the 48-hour treatment period and increased bioavailability due to the nanoparticle formulation [24,60,61].

Table 4. IC-50 of paclitaxel, paclitaxel nanoparticles, lapatinib, and lapatinib nanoparticles in OVCA-432 cells.

Drug Treatment	IC-50 (μ _ξ	g/mL) **
	PTX	LAP
Free PTX *	70.6 ± 5.1	-
Free LAP *	-	4.6 ± 1.3
PTX NPs	0.040 ± 0.003	-
LAP NPs	-	0.80 ± 0.26

^{*} In 2% DMSO with full growth medium. ** The average ± standard deviation (n = 6 treatments) are reported.

3.4. Cell Cycle Analysis

To better understand the increase in drug potency upon encapsulation, we examined the effect of treatment on the cell cycle using flow cytometry. The difficulty of treating cancer is the rapid proliferation of tumor cells and the propensity for metastasis. It is vital that cancer treatments such as PTX inhibit proliferation. For example, PTX arrests cells in the G_2/M phase by stabilizing microtubules and preventing their disassembly necessary for cell division [62]. Thus, we examined the effect of the nanoparticles on the cell cycle using flow cytometry. Specifically, we compared the cell cycle of cells treated with free PTX and PTX NPs at their respective IC-50 concentrations. The untreated control cells were primarily in the G_0/G_1 phase with only 9% in the G_2/M phase. With free PTX, the percentage of cells in the G_0/G_1 phase drops from 62% to 45% and there is an increase in the number of cells in the G_2/M phase to 31% (Figure 3A). These results indicate that free PTX formulations accumulate OVCA-432 cells in the G_2/M phase and likely decrease the cell viability by preventing progression to mitosis [62]. LAP and LAP-NP-treated cells remained primarily in the G_0/G_1 phase (Figure 3B) and the proportions for LAP and LAP NPs were comparable. Thus, free LAP and LAP NPs seem to stabilize the cells in the G_0/G_1 phase over the 48-hour treatment with minimal progression to the sub G_1 phase as expected since LAP is known to arrest cancer cells in the G_1 phase of the cell cycle [63].

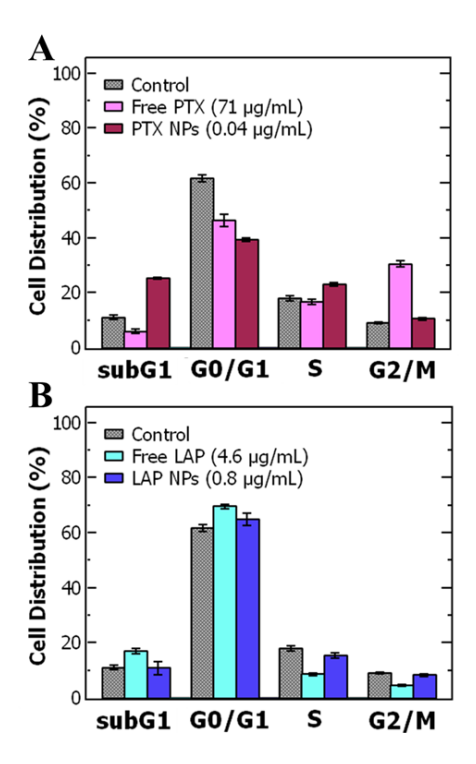


Figure 3. Cell cycle analysis of OVCA-432 cells from flow cytometry to compare free drug (in 2% v/v Figure 3. Cell cycle analysis of OVCA-432 cells from flow cytometry to compare free drug (in 2% v/v Figure 3. Cell cycle analysis of OVCA-432 cells from flow cytometry to compare free drug (in 2% v/v Figure 3. Cell cycle analysis of OVCA-432 cells from flow cytometry to compare free drug (in 2% v/v Figure 3. Cell cycle analysis of OVCA-432 cells from flow cytometry to compare free drug (in 2% v/v Figure 3. Cell cycle analysis of OVCA-432 cells from flow cytometry to compare free drug (in 2% v/v Figure 3. Cell cycle analysis of OVCA-432 cells from flow cytometry to compare free drug (in 2% v/v Figure 3. Cell cycle analysis of OVCA-432 cells from flow cytometry to compare free drug (in 2% v/v Figure 3. Cell cycle analysis of OVCA-432 cells from flow cytometry to compare free drug (in 2% v/v Figure 3. Cell cycle analysis of OVCA-432 cells from flow cytometry to compare free drug (in 2% v/v Figure 3. Cell cycle analysis of OVCA-432 cells from flow cytometry to compare free drug (in 2% v/v Figure 3. Cell cycle analysis of OVCA-432 cells from flow cytometry to compare free drug (in 2% v/v Figure 3. Cell cycle analysis of OVCA-432 cells from flow cytometry to compare free drug (in 2% v/v Figure 3. Cell cycle analysis of OVCA-432 cells from flow cytometry to compare free drug (in 2% v/v Figure 3. Cell cycle analysis of OVCA-432 cells from flow cytometry to compare free drug (in 2% v/v Figure 3. Cell cycle analysis of OVCA-432 cells from flow cytometry to compare free drug (in 2% v/v Figure 3. Cell cycle analysis of OVCA-432 cells from flow cytometry to compare free drug (in 2% v/v Figure 3. Cell cycle analysis of OVCA-432 cells from flow cytometry to compare from flow cytometry to compare free drug (in 2% v/v Figure 3. Cell cycle analysis of OVCA-432 cells from flow cytometry to compare free drug (in 2% v/v Figure 3. Cell cycle analysis of OVCA-432 cells from flow cytometry to cycle analysis of OVCA-432 cells from flow c

While the control nanoparticles had no effect on the cell cycle (Figure S6), when OVCA-432 cells will be the control propertiales had no effect on the cell cycle (Figure S6), when OVCA-432 cells will be the control propertial by the properties of the cells of the School of the PBX tells tell were literated by the properties the cells of the section of the cells of the section of the cells of

- 3.5. Drug Combination and Synergy
- 3.5. Drug Combination and Synergy flicacy of the co-loaded formulation. Co-encapsulating the PTX with LAP furtherestain the PTX with LAP furtherestain the PTX flight 4). LAP further shlitting the PTX flight 4). LAP further increases PTX potency as indicated by the two-fold decrease in IC-50.

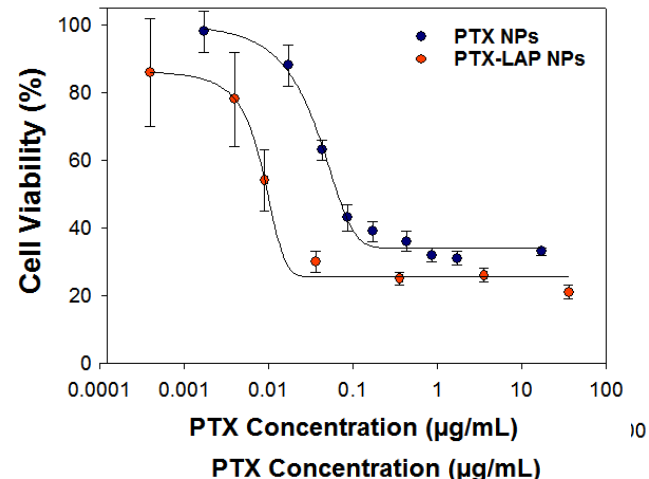


Figure 4. The cell viability dose—response curve of OVCA-432 cells when treated with (blue) paclitaxel national representations of the paclitaxel of the pac

Based on the IC-50 of PTX-LAP NPs, we compared the cell viability of OVCA-432 cells treated with a Based on the IC-50 of PTX-LAP NPs, we compared the cell viability of OVCA-432 cells treated with a Based on the IC-50 of PTX-LAP NPs, we compared the cell viability of OVCA-432 cells treated with a Based on the IC-50 of PTX-LAP NPs we compared the cell viability of OVCA-432 cells treated with a Based on the IC-50 of PTX-LAP NPs as included the IC-50 of IC-41 of IC-50 of

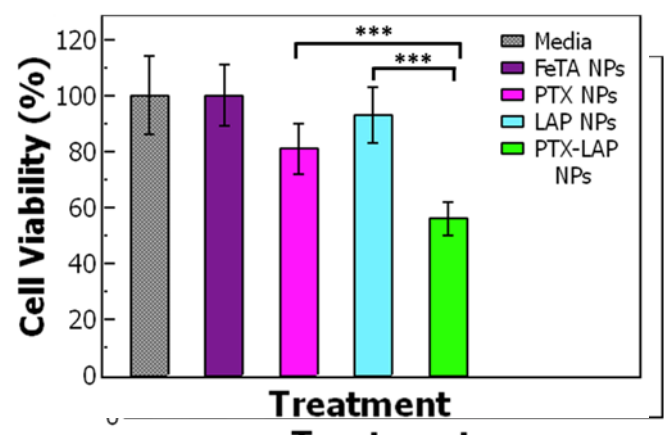


Figure Selection annount of the CATES Constituted for the Cate of the Cate of

Building on these results, we compared the combination treatment to the single-drug treatment to determinate the measure symposition of the treating above the with PTX trading PE. Symposition of the treating above the with PTX trading PE. Symposition of the treating above Tallel and the PTX trading PE. Symposition of the combination index (CI) based on the Chou—Tallel and method and when the CI is

Nanomaterials **2020**, 10, 561

Building on these results, we compared the combination treatment to the single-drug treatment to determine if there was a synergistic effect of co-treating the cells with PTX and LAP. Synergy was examined with the combination index (CI) based on the Chou–Talalay method and when the CI is below one, the combination treatment is synergistic compared to the sum of the individual drug treatments [67–69]. Free PTX and free LAP can be combined synergistically as indicated by the CI of 0.18. PTX and LAP target different mechanisms of the cell to produce an anticancer effect [70,71]. LAP inhibits the function of ABC transporters, which helps increase the intracellular concentration of PTX thereby increasing drug efficacy [24,72,73]. Similar synergistic effects were seen with chemotherapeutic agents and tyrosine kinase inhibitors [12,13].

Interestingly, the CI of the co-loaded PTX–LAP NPs was 0.23 comparable to the free drug combination and lower than co-delivered nanoparticles, which had a CI of 0.40 (Table 5). These results indicate an advantage to the co-encapsulation of both drugs within the same particle. The co-loaded nanoparticles could enhance the co-localization of the drugs particularly if the nanoparticles are endocytosed by tumor cells. Overall, we have presented a rapid and scalable approach to encapsulating chemotherapeutic combinations in a pH-labile nanoparticle platform that enhances the potency treatment of ovarian cancer in vitro.

Table 5. IC-50 and combination index of paclitaxel–lapatinib nanoparticles (PTX–LAP NPs) (co-loaded) compared to simultaneous delivery of paclitaxel nanoparticles (PTX NPs) and lapatinib nanoparticles (LAP NPs) (two single-drug-loaded NPs) in OVCA-432 cells.

Drug Treatment	IC-50 (μg	Combination		
0 —	PTX	LAP	Index (CI)	
PTX NPs and LAP NPs	0.015 ± 0.003	0.007 ± 0.001	0.40	
PTX-LAP NPs	0.0090 ± 0.0009	0.0040 ± 0.0004	0.23	

The average \pm standard deviation from one experiment performed with 6 replicate wells is reported.

4. Conclusions

In conclusion, we demonstrated the encapsulation of weakly hydrophobic drugs (logP < 6) into polymer nanoparticles in a rapid, scalable FNP process using in situ complexation of TA–Fe. The size of the resulting nanoparticles is stable at pH 7.4, facilitating sustained drug release via first-order Fickian diffusion. Importantly, the nanoparticles that encapsulate PTX and LAP are significantly more potent than the free drugs as indicated by the significantly decreased IC-50. Co-encapsulating PTX with LAP further increased potency. Additionally, co-encapsulating PTX and LAP had a synergistic effect compared to the free drug and greater than co-delivery of the single-drug-loaded nanoparticles indicating an advantage co-encapsulation of both drugs within the same particle. Building on this promising study, further studies to understand the cytotoxic effects (e.g., apoptosis), nanoparticle uptake and localization within cells, protein adsorption to nanoparticles, as well as evaluation in additional cell lines will be considered in future work. This is an intriguing approach for improving the potency of existing chemotherapeutics.

Supplementary Materials: The following are available online at http://www.mdpi.com/2079-4991/10/3/561/s1, Figure S1: Overview of nanoparticle self-assembly with Flash NanoPrecipitation; Figure S2: Dynamic light scattering of TA–Fe NPs (containing no drugs); Figure S3: TEM images of PTX NPs and LAP NPs; Figure S4: Dynamic light scattering of LAP NPs; Table S1: Effect of varying drug concentration when preparing PTX–LAP NPs; Table S2: Comparing nanoparticles size and polydispersity before and after filtration; Table S3: Nanoparticles stability; Table S4: Cell Viability of cell treated with Fe-TA NPs; Table S5: Comparing reproducibility of the IC-50 of OVCA-432 cells treated with free PTX; Table S6: Cell viability of cells treated with free PTX and PTX NPs; Figure S5: Dose–response curve for cell treated with free LAP and LAP NPs; Figure S6: Cell cycle distribution of untreated cells and cell treated with TA–Fe NPs.

Author Contributions: Conceptualization, S.L.L., H.Y. and C.T.; formal analysis, S.L.L. and C.T.; funding acquisition, C.T.; investigation, S.L.L.; methodology, S.L.L., H.Y. and C.T.; project administration, C.T.; supervision,

Nanomaterials **2020**, *10*, 561 14 of 17

C.T.; Validation, S.L.L.; writing—original draft preparation, S.L.L. and C.T.; writing—review and editing, S.L.L., H.Y. and C.T. All authors have read and agreed to the published version of the manuscript.

Funding: This work was partially supported by the VCU College of Engineering and NSF (Award Number 1651957).

Acknowledgments: The authors gratefully acknowledge Joseph Turner and Matthew Halquist for instrumental support. Additionally, the authors would like to acknowledge Judy Williamson for assistance with TEM analysis and Julie Farnsworth and Xinyan Pei for assistance with flow cytometry. The authors would also like to acknowledge Remy Cooper and Christopher Vasey for their assistance with experiments. Microscopy was performed at the VCU Microscopy Facility and Flow cytometry was performed at the VCU Flow Cytometer Shared Resource Core, supported, in part, by funding from NIH-NCI Cancer Center Support Grant P30 CA016059.

Conflicts of Interest: The authors declare no conflicts of interest. The funders had no role in the design of the study; in the collection, analyses, or interpretation of data; in the writing of the manuscript, or in the decision to publish the results.

References

- 1. Torre, L.A.; Trabert, B.; DeSantis, C.E.; Miller, K.D.; Samimi, G.; Runowicz, C.D.; Gaudet, M.M.; Jemal, A.; Siegel, R.L. Ovarian cancer statistics, 2018. *Cancer J. Clin.* **2018**, *68*, 284–296. [CrossRef]
- 2. Ueno, N.T.; Mamounas, E.P. Neoadjuvant nab-paclitaxel in the treatment of breast cancer. *Breast Cancer Res. Treat.* **2016**, *156*, 427–440. [CrossRef] [PubMed]
- 3. Sridhar, S.S.; Hotte, S.J.; Chin, J.L.; Hudes, G.R.; Gregg, R.; Trachtenberg, J.; Wang, L.; Tran-Thanh, D.; Pham, N.-A.; Tsao, M.-S.; et al. A multicenter phase II clinical trial of lapatinib (GW572016) in hormonally untreated advanced prostate cancer. *Am. J. Clin. Oncol.* **2010**, *33*, 609–613. [CrossRef] [PubMed]
- 4. Rao, S.; Krauss, N.E.; Heerding, J.M.; Swindell, C.S.; Ringel, I.; Orr, G.A.; Horwitz, S.B. 3'-(p-azidobenzamido)taxol photolabels the N-terminal 31 amino acids of beta-tubulin. *J. Biol. Chem.* 1994, 269, 3132–3134. [PubMed]
- 5. Rao, S.; He, L.; Chakravarty, S.; Ojima, I.; Orr, G.A.; Horwitz, S.B. Characterization of the Taxol binding site on the microtubule. Identification of Arg(282) in beta-tubulin as the site of photoincorporation of a 7-benzophenone analogue of Taxol. *J. Biol. Chem.* 1999, 274, 37990–37994. [CrossRef] [PubMed]
- 6. Schiff, P.B.; Horwitz, S.B. Taxol stabilizes microtubules in mouse fibroblast cells. *Proc. Natl. Acad. Sci. USA* **1980**, 77, 1561–1565. [CrossRef]
- 7. Vergara, D.; Bellomo, C.; Zhang, X.; Vergaro, V.; Tinelli, A.; Lorusso, V.; Rinaldi, R.; Lvov, Y.M.; Leporatti, S.; Maffia, M. Lapatinib/Paclitaxel polyelectrolyte nanocapsules for overcoming multidrug resistance in ovarian cancer. *Nanomedicine* **2012**, *8*, 891–899. [CrossRef]
- 8. Van Zuylen, L.; Verweij, J.; Sparreboom, A. Role of formulation vehicles in taxane pharmacology. *Investig. New Drugs* **2001**, *19*, 125–141. [CrossRef]
- 9. Markman, M.; Kennedy, A.; Webster, K.; Kulp, B.; Peterson, G.; Belinson, J. Phase I Trial of Paclitaxel Plus Megestrol Acetate in Patients with Paclitaxel-refractory Ovarian Cancer. *Clin. Cancer Res.* **2000**, *6*, 4201–4204.
- 10. Varma, M.V.S.; Panchagnula, R. Enhanced oral paclitaxel absorption with vitamin E-TPGS: Effect on solubility and permeability in vitro, in situ and in vivo. *Eur. J. Pharm. Sci.* **2005**, 25, 445–453. [CrossRef]
- 11. Yagi, H.; Yotsumoto, F.; Sonoda, K.; Kuroki, M.; Mekada, E.; Miyamoto, S. Synergistic anti-tumor effect of paclitaxel with CRM197, an inhibitor of HB-EGF, in ovarian cancer. *Int. J. Cancer* **2009**, 124, 1429–1439. [CrossRef] [PubMed]
- 12. Cheng, H.; An, S.-J.; Zhang, X.-C.; Dong, S.; Zhang, Y.-F.; Chen, Z.-H.; Chen, H.-J.; Guo, A.-L.; Lin, Q.-X.; Wu, Y.-L. In vitro sequence-dependent synergism between paclitaxel and gefitinib in human lung cancer cell lines. *Cancer Chemother. Pharmacol.* **2011**, *67*, 637–646. [CrossRef] [PubMed]
- He, X.; Zhang, T. Alteration in the Balance of Prosurvival and Proapoptotic Signalling Pathways Leads to Sequence-Dependent Synergism Between Docetaxel and Sorafenib in Human Non-small Cell Lung Cancer Cell Lines. Cell Biochem. Biophys. 2014, 68, 411–418. [CrossRef] [PubMed]
- 14. Di Leo, A.; Gomez, H.L.; Aziz, Z.; Zvirbule, Z.; Bines, J.; Arbushites, M.C.; Guerrera, S.F.; Koehler, M.; Oliva, C.; Stein, S.H.; et al. Phase III, Double-Blind, Randomized Study Comparing Lapatinib Plus Paclitaxel With Placebo Plus Paclitaxel As First-Line Treatment for Metastatic Breast Cancer. *J. Clin. Oncol.* 2008, 26, 5544–5552. [CrossRef] [PubMed]

Nanomaterials **2020**, *10*, 561 15 of 17

15. Satoh, T.; Xu, R.-H.; Chung, H.C.; Sun, G.-P.; Doi, T.; Xu, J.-M.; Tsuji, A.; Omuro, Y.; Li, J.; Wang, J.-W.; et al. Lapatinib plus paclitaxel versus paclitaxel alone in the second-line treatment of HER2-amplified advanced gastric cancer in Asian populations: TyTAN—A randomized, phase III study. *J. Clin. Oncol.* **2014**, 32, 2039–2049. [CrossRef] [PubMed]

- 16. Martin, L.; Schilder, R. Novel Approaches in Advancing the Treatment of Epithelial Ovarian Cancer: The Role of Angiogenesis Inhibition. *J. Clin. Oncol.* **2007**, *25*, 2894–2901. [CrossRef]
- 17. Teplinsky, E.; Muggia, F. Targeting HER2 in ovarian and uterine cancers: Challenges and future directions. *Gynecol. Oncol.* **2014**, *135*, 364–370. [CrossRef]
- 18. Kondo, N.; Tsukuda, M.; Ishiguro, Y.; Kimura, M.; Fujita, K.; Sakakibara, A.; Takahashi, H.; Toth, G.; Matsuda, H. Antitumor effects of lapatinib (GW572016), a dual inhibitor of EGFR and HER-2, in combination with cisplatin or paclitaxel on head and neck squamous cell carcinoma. *Oncol. Rep.* **2010**, *23*, 957–963. [CrossRef]
- 19. Guo, X.; Li, S.; Zhu, X.; Dou, Q.; Liu, D. Lapatinib in combination with paclitaxel plays synergistic antitumor effects on esophageal squamous cancer. *Cancer Chemother. Pharmacol.* **2018**, *82*, 383–394. [CrossRef]
- 20. Weiss, R.B.; Donehower, R.C.; Wiernik, P.H.; Ohnuma, T.; Gralla, R.J.; Trump, D.L.; Baker, J.R.; Van Echo, D.A.; Von Hoff, D.D.; Leyland-Jones, B. Hypersensitivity reactions from taxol. *J. Clin. Oncol.* **1990**, *8*, 1263–1268. [CrossRef]
- 21. Schiller, J.H.; Harrington, D.; Belani, C.P.; Langer, C.; Sandler, A.; Krook, J.; Zhu, J.; Johnson, D.H. Comparison of Four Chemotherapy Regimens for Advanced Non–Small-Cell Lung Cancer. *N. Engl. J. Med.* **2002**, *346*, 92–98. [CrossRef] [PubMed]
- 22. Peer, D.; Karp, J.M.; Hong, S.; Farokhzad, O.C.; Margalit, R.; Langer, R. Nanocarriers as an emerging platform for cancer therapy. *Nat. Nanotechnol.* **2007**, 2, 751–760. [CrossRef] [PubMed]
- 23. Yeh, T.K.; Lu, Z.; Wientjes, M.G.; Au, J.L.-S. Formulating Paclitaxel in Nanoparticles Alters Its Disposition. *Pharm. Res.* **2005**, 22, 867–874. [CrossRef] [PubMed]
- 24. Li, F.; Danquah, M.; Singh, S.; Wu, H.; Mahato, R.I. Paclitaxel- and lapatinib-loaded lipopolymer micelles overcome multidrug resistance in prostate cancer. *Drug Deliv. Transl. Res.* **2011**, *1*, 420–428. [CrossRef]
- 25. Wei, Y.; Xu, S.; Wang, F.; Zou, A.; Zhang, S.; Xiong, Y.; Cao, S.; Zhang, Q.; Wang, Y.; Jiang, X. A Novel Combined Micellar System of Lapatinib and Paclitaxel with Enhanced Antineoplastic Effect Against Human Epidermal Growth Factor Receptor-2 Positive Breast Tumor In Vitro. *J. Pharm. Sci.* 2015, 104, 165–177. [CrossRef] [PubMed]
- 26. Ravar, F.; Saadat, E.; Kelishadi, P.D.; Dorkoosh, F.A. Liposomal formulation for co-delivery of paclitaxel and lapatinib, preparation, characterization and optimization. *J. Liposome Res.* **2016**, *26*, 175–187. [CrossRef]
- 27. Dehghankelishadi, P.; Saadat, E.; Ravar, F.; Safavi, M.; Pordeli, M.; Gholami, M.; Dorkoosh, F.A. In vitro and in vivo evaluation of paclitaxel–lapatinib-loaded F127 pluronic micelles. *Drug Dev. Ind. Pharm.* **2017**, 43, 390–398. [CrossRef]
- 28. Pinkerton, N.M.; Grandeury, A.; Fisch, A.; Brozio, J.; Riebesehl, B.U.; Prud'homme, R.K. Formation of Stable Nanocarriers by in Situ Ion Pairing during Block-Copolymer-Directed Rapid Precipitation. *Mol. Pharm.* **2013**, 10, 319–328. [CrossRef]
- 29. Ganta, S.; Amiji, M. Coadministration of Paclitaxel and curcumin in nanoemulsion formulations to overcome multidrug resistance in tumor cells. *Mol. Pharm.* **2009**, *6*, 928–939. [CrossRef]
- 30. Kelishady, P.D.; Saadat, E.; Ravar, F.; Akbari, H.; Dorkoosh, F. Pluronic F127 polymeric micelles for co-delivery of paclitaxel and lapatinib against metastatic breast cancer: Preparation, optimization and in vitro evaluation. *Pharm. Dev. Technol.* **2015**, 20, 1009–1017. [CrossRef]
- 31. Duong, A.D.; Ruan, G.; Mahajan, K.; Winter, J.O.; Wyslouzil, B.E. Scalable, semicontinuous production of micelles encapsulating nanoparticles via electrospray. *Langmuir* **2014**, *30*, 3939–3948. [CrossRef] [PubMed]
- 32. Tang, C.; Prud'homme, R.K. Targeted Theragnostic Nanoparticles via Flash Nanoprecipitation: Principles of Material Selection. In *Polymer Nanoparticles for Nanomedicines*; Springer: Cham, Switzerland, 2016; pp. 55–85. ISBN 978-3-319-41419-5.
- 33. Pustulka, K.M.; Wohl, A.R.; Lee, H.S.; Michel, A.R.; Han, J.; Hoye, T.R.; McCormick, A.V.; Panyam, J.; Macosko, C.W. Flash nanoprecipitation: Particle structure and stability. *Mol. Pharm.* **2013**, *10*, 4367–4377. [CrossRef] [PubMed]
- 34. Levit, S.L.; Stwodah, R.M.; Tang, C. Rapid, Room Temperature Nanoparticle Drying and Low-Energy Reconstitution via Electrospinning. *J. Pharm. Sci.* **2018**, *107*, 807–813. [CrossRef] [PubMed]

Nanomaterials **2020**, *10*, 561 16 of 17

35. Tang, C.; Amin, D.; Messersmith, P.B.; Anthony, J.E.; Prud'homme, R.K. Polymer Directed Self-Assembly of pH-Responsive Antioxidant Nanoparticles. *Langmuir* 2015, *31*, 3612–3620. [CrossRef] [PubMed]

- 36. Han, J.; Zhu, Z.; Qian, H.; Wohl, A.R.; Beaman, C.J.; Hoye, T.R.; Macosko, C.W. A simple confined impingement jets mixer for flash nanoprecipitation. *J. Pharm. Sci.* 2012, 101, 4018–4023. [CrossRef] [PubMed]
- 37. *Understanding the Colloidal Stability of Protein Therapeutics Using Dynamic Light Scattering*; Malvern Instruments Limited: Malvern, UK, 2014.
- 38. Han, J.; Michel, A.R.; Lee, H.; Kalscheuer, S.; Wohl, A.; Hoye, T.R.; McCormick, A.V.; Panyam, J.; Macosko, C. Nanoparticles Containing High Loads of Paclitaxel-Silicate Prodrugs: Formulation, Drug Release, and Anticancer Efficacy. *Curr. Heart Fail. Rep.* **2015**, 12, 4329–4335. [CrossRef]
- 39. Pagels, R.F.; Edelstein, J.; Tang, C.; Prud'homme, R.K. Controlling and Predicting Nanoparticle Formation by Block Copolymer Directed Rapid Precipitations. *Nano Lett.* **2018**, *18*, 1139–1144. [CrossRef]
- 40. Tang, C.; Sosa, C.L.; Pagels, R.F.; Priestley, R.D.; Prud'homme, R.K. Efficient preparation of size tunable PEGylated gold nanoparticles. *J. Mater. Chem. B* **2016**, *4*, 4813–4817. [CrossRef]
- 41. Tang, C.; Levit, S.; Zeevi, M.; Vasey, C.; Fromen, C. Chapter 12: Polymer Colloids Enable Medical Applications. In *Polymer Colloids: Formulation, Characterization, and Applications*; Royal Society of Chemistry: Cambridge, UK, 2019; pp. 358–398.
- 42. Johnson, B.K.; Prud homme, R.K. Flash NanoPrecipitation of Organic Actives and Block Copolymers using a Confined Impinging Jets Mixer. *Aust. J. Chem.* **2003**, *56*, 1021–1024. [CrossRef]
- 43. Zajdel, A.; Wilczok, A.; Jelonek, K.; Musiał-Kulik, M.; Foryś, A.; Li, S.; Kasperczyk, J. Cytotoxic Effect of Paclitaxel and Lapatinib Co-Delivered in Polylactide-co-Poly(ethylene glycol) Micelles on HER-2-Negative Breast Cancer Cells. *Pharmaceutics* **2019**, *11*, 169. [CrossRef]
- 44. Jia, L.; Shen, J.; Li, Z.; Zhang, D.; Zhang, Q.; Liu, G.; Zheng, D.; Tian, X. In vitro and in vivo evaluation of paclitaxel-loaded mesoporous silica nanoparticles with three pore sizes. *Int. J. Pharm.* **2013**, 445, 12–19. [CrossRef] [PubMed]
- 45. Chavanpatil, M.D.; Patil, Y.; Panyam, J. Susceptibility of nanoparticle-encapsulated paclitaxel to P-glycoprotein-mediated drug efflux. *Int. J. Pharm.* **2006**, 320, 150–156. [CrossRef]
- 46. Modi, S.; Anderson, B.D. Determination of Drug Release Kinetics from Nanoparticles: Overcoming Pitfalls of the Dynamic Dialysis Method. *Mol. Pharm.* **2013**, *10*, 3076–3089. [CrossRef] [PubMed]
- 47. D'Souza, S.S.; DeLuca, P.P. Methods to Assess in Vitro Drug Release from Injectable Polymeric Particulate Systems. *Pharm. Res.* **2006**, 23, 460–474. [CrossRef] [PubMed]
- 48. Dash, S.; Murthy, P.N.; Nath, L.; Chowdhury, P. Kinetic modeling on drug release from controlled drug delivery systems. *Acta Pol. Pharm.* **2010**, *67*, 217–223. [PubMed]
- 49. Korsmeyer, R.W.; Gurny, R.; Doelker, E.; Buri, P.; Peppas, N.A. Mechanisms of solute release from porous hydrophilic polymers. *Int. J. Pharm.* **1983**, *15*, 25–35. [CrossRef]
- 50. Gillespie, D.T.; Seitaridou, E. *Simple Brownian Diffusion: An Introduction to the Standard Theoretical Models*; Oxford University Press: Oxford, NY, USA, 2012; ISBN 978-0-19-966450-4.
- 51. Wu, I.Y.; Bala, S.; Škalko-Basnet, N.; di Cagno, M.P. Interpreting non-linear drug diffusion data: Utilizing Korsmeyer-Peppas model to study drug release from liposomes. *Eur. J. Pharm. Sci.* **2019**, *138*, 105026. [CrossRef]
- 52. Liu, P.; De Wulf, O.; Laru, J.; Heikkilä, T.; van Veen, B.; Kiesvaara, J.; Hirvonen, J.; Peltonen, L.; Laaksonen, T. Dissolution Studies of Poorly Soluble Drug Nanosuspensions in Non-sink Conditions. *AAPS PharmSciTech* **2013**, *14*, 748–756. [CrossRef]
- 53. Mobasseri, R.; Karimi, M.; Tian, L.; Naderi-Manesh, H.; Ramakrishna, S. Hydrophobic lapatinib encapsulated dextran-chitosan nanoparticles using a toxic solvent free method: Fabrication, release property & in vitro anti-cancer activity. *Mater. Sci. Eng. C* **2017**, *74*, 413–421.
- 54. Bullock, J. Dissolution of Nanoparticle Drug Formulations. In *Poorly Soluble Drugs: Dissolution and Drug Release*; Taylor & Francis Group: Abingdon, UK, 2017; pp. 325–376. ISBN 9781315364537.
- 55. D'Addio, S.M.; Bukari, A.A.; Dawoud, M.; Bunjes, H.; Rinaldi, C.; Prud'homme, R.K. Determining drug release rates of hydrophobic compounds from nanocarriers. *Philos. Trans. A Math. Phys. Eng. Sci.* **2016**, 374. [CrossRef]
- 56. Gülçin, İ.; Huyut, Z.; Elmastaş, M.; Aboul-Enein, H.Y. Radical scavenging and antioxidant activity of tannic acid. *Arab. J. Chem.* **2010**, *3*, 43–53. [CrossRef]

Nanomaterials **2020**, 10, 561

57. Varbiro, G.; Veres, B.; Gallyas, F.; Sumegi, B. Direct effect of Taxol on free radical formation and mitochondrial permeability transition. *Free Rad. Biol. Med.* **2001**, *31*, 548–558. [CrossRef]

- 58. Fonseca, C.; Simões, S.; Gaspar, R. Paclitaxel-loaded PLGA nanoparticles: Preparation, physicochemical characterization and in vitro anti-tumoral activity. *J. Control. Release* **2002**, *83*, 273–286. [CrossRef]
- 59. Lee, Y.; Graeser, R.; Kratz, F.; Geckeler, K.E. Paclitaxel-Loaded Polymer Nanoparticles for the Reversal of Multidrug Resistance in Breast Cancer Cells. *Adv. Funct. Mater.* **2011**, *21*, 4211–4218. [CrossRef]
- 60. Hirota, K.; Ter, H. Endocytosis of Particle Formulations by Macrophages and Its Application to Clinical Treatment. In *Molecular Regulation of Endocytosis*; Ceresa, B., Ed.; InTech: London, UK, 2012; ISBN 978-953-51-0662-3.
- 61. Swanson, J.A.; Watts, C. Macropinocytosis. Trends Cell Biol. 1995, 5, 424–428. [CrossRef]
- 62. Shu, C.-H.; Yang, W.K.; Shih, Y.-L.; Kuo, M.-L.; Huang, T.-S. Cell cycle G2/M arrest and activation of cyclin-dependent kinases associated with low-dose paclitaxel-induced sub-G1 apoptosis. *Apoptosis* **1997**, 2, 463–470. [CrossRef]
- 63. Tang, L.; Wang, Y.; Strom, A.; Gustafsson, J.-Å.; Guan, X. Lapatinib induces p27Kip1-dependent G₁ arrest through both transcriptional and post-translational mechanisms. *Cell Cycle* **2013**, *12*, 2665–2674. [CrossRef]
- 64. Wang, T.-H.; Wang, H.-S.; Soong, Y.-K. Paclitaxel-induced cell death. Cancer 2000, 88, 2619–2628. [CrossRef]
- 65. Demidenko, Z.N.; Kalurupalle, S.; Hanko, C.; Lim, C.; Broude, E.; Blagosklonny, M.V. Mechanism of G1-like arrest by low concentrations of paclitaxel: Next cell cycle p53-dependent arrest with sub G1 DNA content mediated by prolonged mitosis. *Oncogene* **2008**, *27*, 4402–4410. [CrossRef]
- 66. Hsiao, J.-R.; Leu, S.-F.; Huang, B.-M. Apoptotic mechanism of paclitaxel-induced cell death in human head and neck tumor cell lines. *J. Oral. Pathol. Med.* **2009**, *38*, 188–197. [CrossRef]
- 67. Chou, T.-C. Drug combination studies and their synergy quantification using the Chou-Talalay method. *Cancer Res.* **2010**, *70*, 440–446. [CrossRef]
- 68. Azmi, A.S.; Banerjee, S.; Ali, S.; Wang, Z.; Bao, B.; Beck, F.W.J.; Maitah, M.; Choi, M.; Shields, T.F.; Philip, P.A.; et al. Network Modeling of MDM2 Inhibitor-Oxaliplatin Combination Reveals Biological Synergy in wt-p53 solid tumors. *Oncotarget* 2011, 2, 378–392. [CrossRef] [PubMed]
- 69. Ashton, J.C. Drug Combination Studies and Their Synergy Quantification Using the Chou–Talalay Method—Letter. *Cancer Res.* **2015**, *75*, 2400. [CrossRef] [PubMed]
- 70. Rowinsky, E.K.; Donehower, R.C. Paclitaxel (Taxol). N. Engl. J. Med. 1995, 332, 1004–1014. [CrossRef]
- 71. Moy, B.; Kirkpatrick, P.; Kar, S.; Goss, P. Lapatinib. Nat. Rev. Drug Discov. 2007, 6, 431–432. [CrossRef]
- 72. Dai, C.; Tiwari, A.K.; Wu, C.-P.; Su, X.; Wang, S.-R.; Liu, D.; Ashby, C.R.; Huang, Y.; Robey, R.W.; Liang, Y.; et al. Lapatinib (Tykerb, GW572016) Reverses Multidrug Resistance in Cancer Cells by Inhibiting the Activity of ATP-Binding Cassette Subfamily B Member 1 and G Member 2. *Cancer Res.* 2008, 68, 7905–7914. [CrossRef]
- 73. Dai, C.; Ma, S.; Wang, F.; Zhao, H.; Wu, X.; Huang, Z.; Chen, Z.; To, K.; Fu, L. Lapatinib promotes the incidence of hepatotoxicity by increasing chemotherapeutic agent accumulation in hepatocytes. *Oncotarget* **2015**, *6*, 17738–17752. [CrossRef]



© 2020 by the authors. Licensee MDPI, Basel, Switzerland. This article is an open access article distributed under the terms and conditions of the Creative Commons Attribution (CC BY) license (http://creativecommons.org/licenses/by/4.0/).